Supporting Information

On the origin of the difference between type A and type B skeletal isomerization of alkenes catalyzed by zeolites: the crucial input of ab initio molecular dynamics

Jérôme Rey,[1] Axel Gomez,[1] Pascal Raybaud,[1] Céline Chizallet,[1,] Tomáš Bučko,[2,3]**

[1] IFP Energies nouvelles – Rond-Point de l'Echangeur de Solaize – BP 3 69360 Solaize, France

[2] Department of Physical and Theoretical Chemistry, Faculty of Natural Sciences, Comenius University in Bratislava, Ilkovičova 6, SK- 84215 Bratislava, Slovakia

[3]Institute of Inorganic Chemistry, Slovak Academy of Sciences, Dúbravská cesta 9, SK-84236 Bratislava, Slovakia

Corresponding authors: celine.chizallet@ifpen.fr ; bucko19@uniba.sk

SI. Probability distribution functions $\widetilde{P}(\xi)$ for reactant and product states of type A and B isomerizations

In this section we provide probability densities $\tilde{P}(\xi)$ for the reaction coordinate ξ computed using straightforward molecular dynamics (Figures S1, S2, S3) for the reactant and product configurations of isomerization B and A. The values of $\tilde{P}(\xi_{ref})$ employed in the free energy calculations (see Equations (1) and (2) in the main text), discussed in Sections 3.3.2 and 3.4.2 in the main text, are listed in Table S1. In each case, the reference state ξ_{ref} was chosen such that the corresponding value of probability density was sufficiently high so that it could be determined with a good accuracy. We emphasize that the particular choice of value of ξ_{ref} does not affect the numerical results of the free energy calculations (provided the value of $\tilde{P}(\xi_{ref})$ is sufficiently accurate). Note that Figures S2 and S3 show distributions for the same chemical species but for different approximation to reaction coordinate (see Sections 3.3.1 and 3.4.1 in the main text).

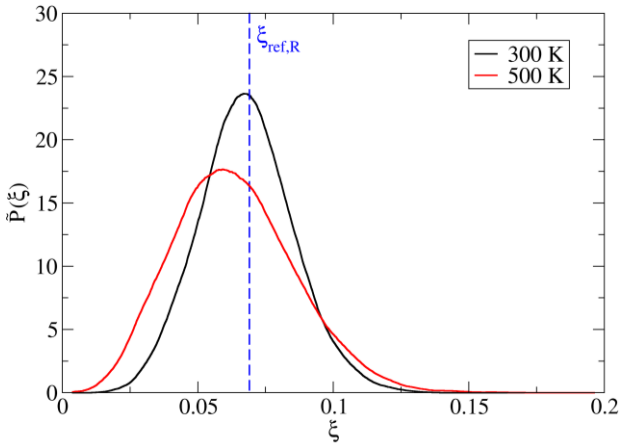

Figure S1. Probability distribution function $\tilde{P}(\xi)$ computed for the reactant state R(I) of type B isomerization at 300 K and 500 K.

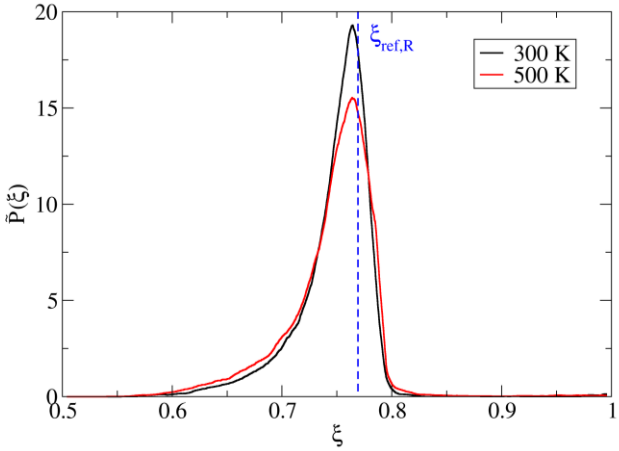

Figure S2. Probability distribution function $\tilde{P}(\xi)$ computed for the product state P of type B isomerization at 300 K and 500 K. The approximation to reaction coordinate (ξ) has been chosen as described in Section 3.3.1 in the main text.

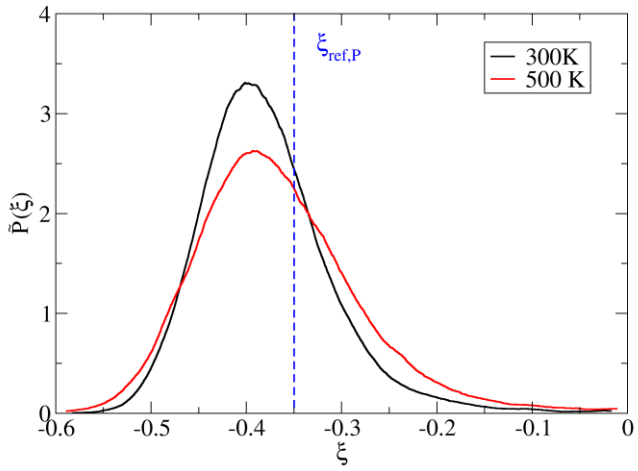

Figure S3. Probability distribution function $\tilde{P}(\xi)$ computed for the reactant/product state P of type A isomerization at 300 K and 500 K. The approximation to reaction coordinate (ξ) has been chosen as described in Section 3.4.1 in the main text.

Table S1. Values of ξ_{ref} for the reactant and product states of type A and B isomerizations, and the corresponding values of probability density ($\tilde{P}(\xi_{ref})$. The lengths of production runs of MD simulations (τ) used to compute $\tilde{P}(\xi_{ref})$ are also listed. As different approximations to reaction coordinate were used in calculations of free energies of both reactions, the values of ξ_{ref} and $\tilde{P}(\xi_{ref})$ listed for the product of type B isomerization and reactant/product of type A isomerization are different although all these states are chemically identical.

	Type B isomerization			
	T (K)	τ (ps)	ξ_{ref}	$\tilde{P}(\xi_{ref})$
Reactant R(I)	300	195	0.069	23.5
	500	195	0.069	16.3
Product P	300	109	0.769	17.9
	500	161	0.769	14.9
	Type A isomerization			
Reactant/product P	300	109	–0.35	2.45
	500	161	–0.35	2.25

SII. Determination of the velocity term $|\dot{\xi}^*|$

The determination of free energies of activation according to the Equation 1 presented in the main text requires the knowledge of average generalized velocity of reaction coordinate at the transition state ($\langle|\dot{\xi}^*|\rangle$). In our calculations, this term is determined using the constrained MD simulations via the formula [1]:

$$\langle|\dot{\xi}^*|\rangle = \frac{\left\langle Z^{-1/2}|\dot{\xi}|\right\rangle_{\xi^*}}{\left\langle Z^{-1/2}\right\rangle_{\xi^*}}, \qquad \text{(Eq. S1)}$$

where the term enclosed in $\langle ... \rangle_{\xi^*}$ is computed as a statistical average for a constrained ensemble with $\xi(\boldsymbol{r}) = \xi^*$, the mass metric tensor is:

$$Z = \sum_{i=1}^{N} \frac{1}{m_i} \sum_{\mu=x,y,z} \left(\frac{\partial \xi}{\partial r_{i,\mu}}\right)^2, \qquad \text{(Eq. S2)}$$

and $\dot{\xi}$ is defined as follows:

$$\dot{\xi} = \sum_{i=1}^{N} \sum_{\mu=x,y,z} \frac{\partial \xi}{\partial r_{i,\mu}} \dot{r}_{i,\mu}, \qquad \text{(Eq. S3)}$$

with $r_{i,\mu}$ being the Cartesian component μ of position vector of an atom i and the sums are over all atoms and Cartesian components. In our calculations, the value of $\left|\dot{\xi}^*\right|$ is computed for 1000 configurations generated by constrained MD with $\xi(\boldsymbol{r}) = \xi^*$ and 500 sets of vectors $\dot{r}$ generated randomly according to the Maxwell-Boltzmann distribution law.

SIII. Avoiding the by-reactions

In our MD simulations, several undesired by-reactions could possibly occur, which would cause severe problems in the free energy calculations. First of all, both reactions considered in this work can be described as transformations of molecular cations created through the protonation of alkenes by Brønsted acid sites of zeolite. Although the cations representing reactants and products indeed correspond to true minima on potential energy surface (as thoroughly verified in Section 3.2. of the main text), the thermal atomic motion might occasionally lead to deprotonation of cations because this undesired process is fast (i.e. linked with a relatively small free energy barrier) compared to the reactions studied in this work. In order to avoid this problem, which is most likely to occur in constrained MD simulations of unstable reaction intermediate states, a restraining potential of the following form:

$$V(R) = \frac{1}{2}K(R - R_0)^2 \qquad \text{(Eq. S4)}$$

has been added to reinforce all C-H bonds involving hydrogen atoms which are not directly involved in the reaction of interest (all 15 C-H bonds in the case of type A isomerization and 14 C-H bonds (all C-H bonds except of that involving the atom H^a, see Figure 1 in the main text) in type B isomerization). In Equation S4, R stands for the interatomic bonding distance C-H, R_0 =1.1 Å corresponds approximately to the equilibrium length of the C-H bond, and the force constant K is set to 100 eV.Å^{-2}.

Another undesired process that could occur in the case of type B isomerization is a transformation of rotational isomer R(I) into R(II) (Figure 3). As only R(I) can directly undergo the atomic rearrangement linked with type B isomerization, it was necessary to avoid such an uncontrolled transformation between stable rotamers in our blue moon sampling simulations (as explained in Section 3.3.2 in the main text, the contribution of state R(II) to free energy of activation is accounted for via $P(\xi_{ref})$). To this end, a smeared step potential (shown in Figure S4) acting on torsional angle H^a–C^4–C^3-C^2 (τ) (see Figure 1 in the main text for labeling of atoms) was added in the constrained simulations where R(I) was present. The form of potential was as follows:

$$V(\tau) = \sum_{i=1}^{2} \frac{A_i}{1 + exp\left(-D_i\left(\frac{\tau}{\tau_{0,i}} - 1\right)\right)}, \qquad \text{(Eq. S5)}$$

where the parameters were set to the following values: $A_1 = A_2 = -2$ eV, $D_1 = D_2 = 20$, $\tau_{0,1}$ =120 deg., and $\tau_{0,2}$ =240 deg. (cf. Figure 4 in the main text). As obvious from Figure S4, the restraining potential is nearly perfectly flat in the region characteristic for R(I) ($\tau \approx 180$ deg.). The extra forces acting on atoms of R(I) due to the presence of $V(\tau)$ are therefore negligible unless a fluctuation attempting the R(I) →R(II) transformation occurs.

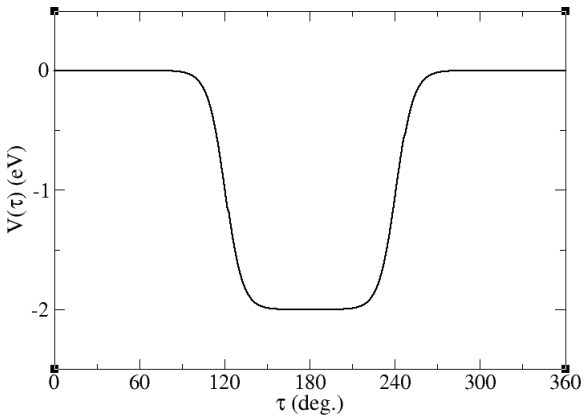

Figure S4. Restraining potential acting on the torsional angle H^a–C^4–C^3-C^2 (τ).

A similar potential (shown in Figure S5) has also been used to act on dihedral angle C^3-C^2-C^4-C^5 (θ) of the states on the product side of type B isomerization in constrained MD simulations which effectively prevented rotations of the three CH_3 groups attached to C^2 around the C^2-C^4 bond. In this case, such a restrain was needed because of the choice of the approximation of the reaction coordinate, which is not invariant with respect to the interchange of methyl groups (see Section 3.3.2 in the main text). The restraining potential has the same form as Eq. S5 and its parameters are set as follows: $A_1 = 2$ eV, $A_2 = -2$ eV, $D_1 = D_2 = 100$, $\tau_{0,1} = -113$ deg., and $\tau_{0,2} = -67$ deg. In this way, the dihedral angle θ was restricted to the values of about –90 deg. characteristic for this particular rotational isomer of the product molecule. Once again, the restraining potential is nearly perfectly flat in the region characteristic for the rotamer of interest and hence the forces due to the restraining potential are negligible unless transition to other rotamer is attempted.

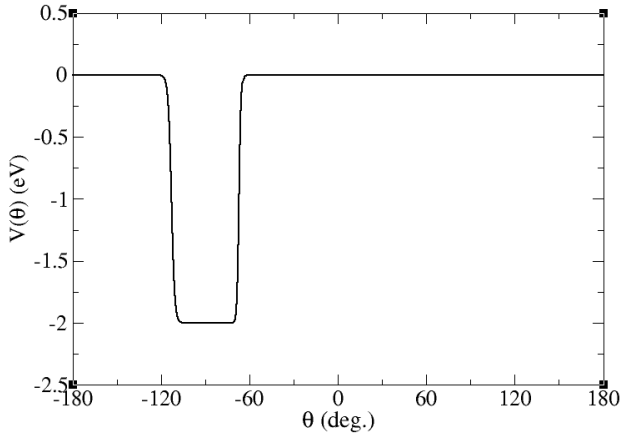

Figure S5. Restraining potential acting on the dihedral angle C^3-C^2-C^4-C^5 (θ).

SIV. Validation of the approximation to reaction coordinate

In this section, we describe the tests performed to validate our choice of the approximation to reaction coordinates.

First, a slow growth simulation protocol (MD in which a candidate CV is increased at a constant rate) has been employed to make sure that the candidate CV can indeed drive smoothly the reaction of interest – from the reactant to the product state and back. The fact that, despite a finite transformation rate, a negligible hysteresis was observed (see Figure S6) is already a good indication of reversibility of the process driven by the given CV. These simulations, that we use solely for the purpose of a qualitative analysis, are performed with a run of length of about 20 ps.

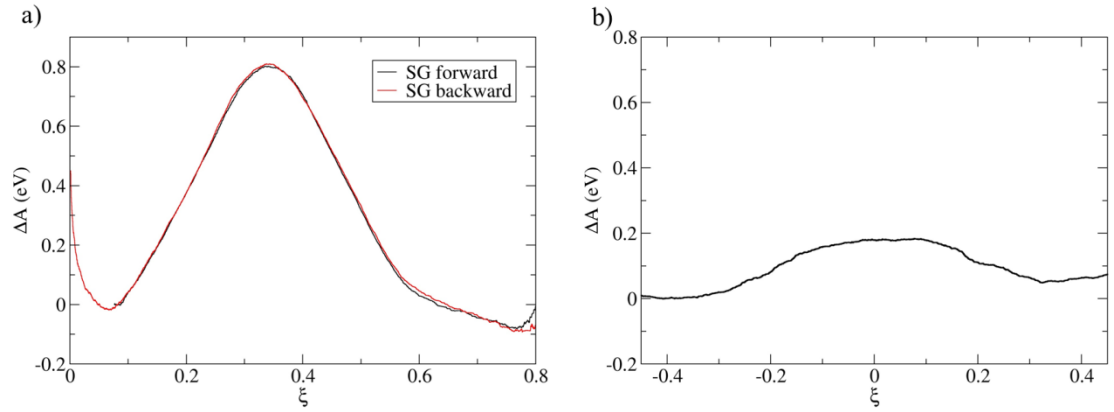

Figure S6. Slow growths simulations for a) the type B isomerization (in gas phase) and b) the type A isomerization (in chabazite).

Second, the distribution of free energy gradients has been monitored for all points along the CV used in the blue moon simulation. As it follows from Figure 1.18 of reference [2] or Figure 1 of reference [3], an incorrect CV would lead to a two-modal distribution of contributions to free energy gradients computed for a point near the separatrix (which follows from the fact that, in such a case, the free energy computed for the subspace of the configurational space orthogonal to CV would have two (or more) minima). In contrast, a correct CV must yield a unimodal distribution at the same point (because there is only one free energy minimum in the subspace spanned by all coordinates orthogonal to CV). As shown in Figure S7, the free energy gradients evaluated for the free energy transition states (and also for all other points) of both reactions studied in our work exhibit a correct behavior.

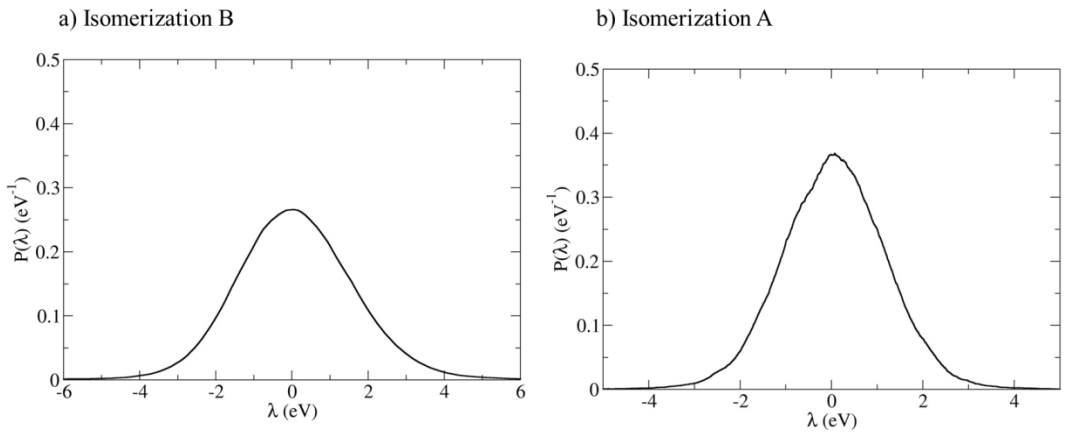

Figure S7. Probability distribution function of the Lagrange multiplier λ associated with the reaction coordinate for the transition states of a) type B isomerization and b) type A isomerization, at 300 K. The Lagrange multiplier λ is the main component of the free-energy gradient [1,4,5]. We note that the approximation to reaction coordinates used in our simulations are dimensionless. The unimodal shape of distributions indicates that our CV corresponds to the case where the reaction is correctly described by the CV [2,3].

Third, an uncontrolled process would be identified by a presence of discontinuity in computed free energy gradients where a small variation in CV would cause a large change in gradient (usually accompanied by a change of its sign). We carefully monitored the free energy gradients computed in our blue moon simulations and, as shown in Figure S8, they do not show any trace of such a discontinuity (besides a small numerical noise due to the statistical uncertainty given by the finite simulation time). Finally, the correctness of our choice is evident also from the semi-quantitative agreement with the static gas phase reactions for which, arguably, the "static" approach represents a more reasonable choice than for the reaction in zeolite.

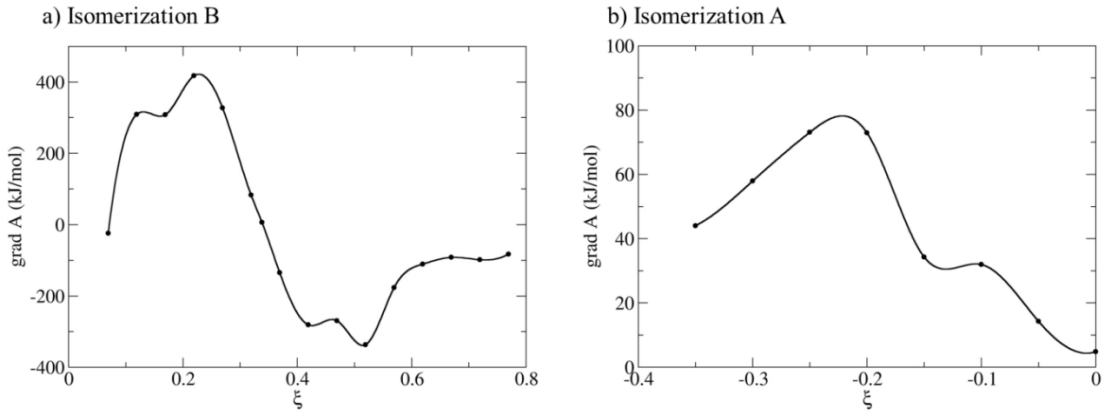

Figure S8. Free energy gradients computed in our blue moon simulations, for a) isomerization B and b) isomerization A. For type A isomerization, the gradient is plotted for $\xi < 0$, the free energy A being an even function by symmetry of reactant and product. We note that the approximation to reaction coordinates used in our simulations are dimensionless, hence the units of gradients.

SV. Static calculations of the gas phase reactions

SV.1. Type B isomerization

Figure S9 shows potential energy of reactant R as a function of torsional and bonding angles τ = H^a–C^4–C^3-C^2 and α =C^4-C^3-C^2 (see Figure 1 for the numbering of atoms) with minima representing two equivalent rotational isomers R(II) ($\tau = \pm 59$ deg.) and the rotamer R(III) ($\tau = 0$ deg.). As evident, the angle α in the isomer R(III) takes much smaller value (~93 deg.) than in R(II) (~106 deg.) or R(I) (~109 deg.). The thermal motion of atoms at the finite temperature MD simulation of R(III) with τ fixed at 0 deg. has a tendency to increase the average value of α to 102-106 deg. depending on the temperature (see Figure S10). According to Figure S9, the system is in a state which is higher in energy compared to R(II) where α assumes a similar value. Consequently, the system naturally relaxes to R(II) if the constraint on τ is removed. This effect explains why R(III) is found to be unstable in our MD simulations (see Section 3.3.2 in the main text).

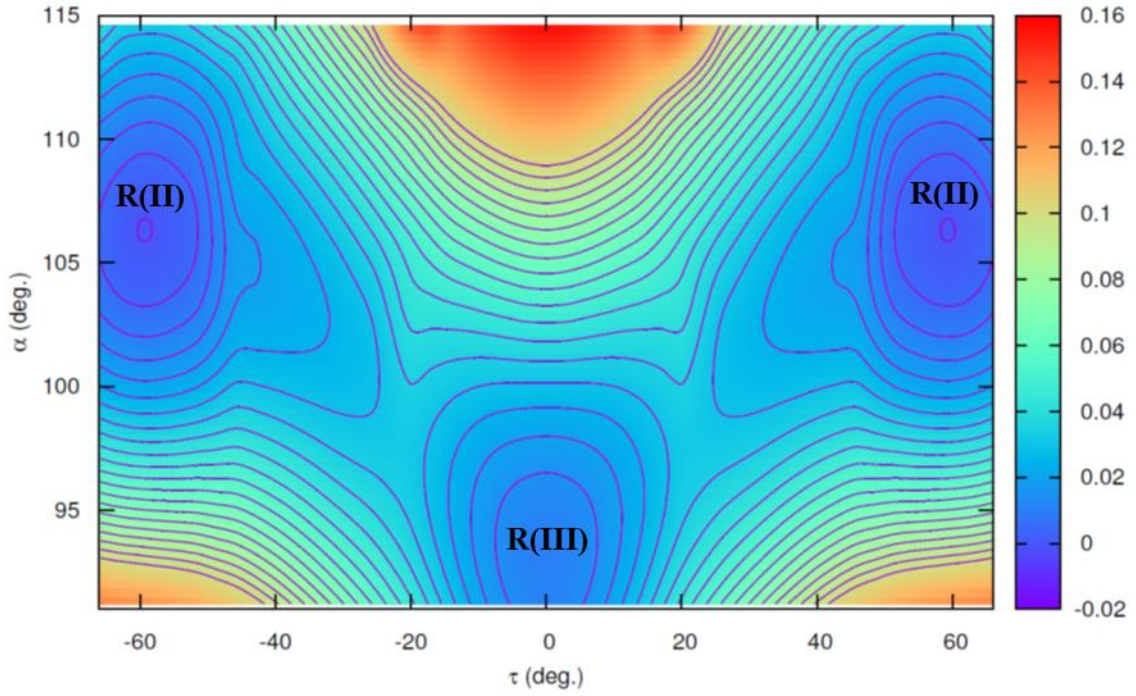

Figure S9. Potential energy of reactant of isomerization B as a function of torsional and bonding angles τ = H^a–C^4–C^3-C^2 and α =C^4-C^3-C^2. The isoenergetic levels are in eV.

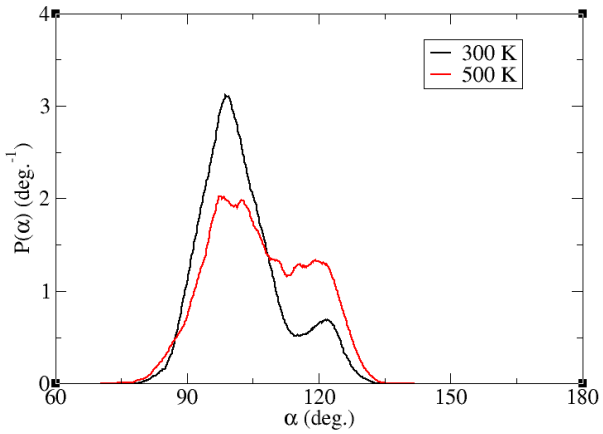

Figure S10. Probability distribution function $P(\alpha)$ for the rotamer R(III) in zeolite at 300 K and 500 K.

Table S2. Helmholtz free energies computed using the static approach for three different rotamers of reactant molecule (R(I), R(II), and R(III)), transition state (TS), and product of type B isomerization reaction of 2,4-dimethyl-pent-2-enium cation in the gas phase. Contributions of the electronic (A_{el}), vibrational (A_{vib}), rotational (A_{rot}), and translational (A_{trans}) degrees of freedom to the total free energy (A_{tot}) of each state at 300 K and 500 K are indicated. All values are in kJ/mol.

	A_{el}	300 K				500 K			
		A_{vib}	A_{rot}	A_{trans}	A_{tot}	A_{vib}	A_{rot}	A_{trans}	A_{tot}
R(I)	-11000.6	499.9	-31.2	-43.6	-10575.6	467.6	-55.2	-78.0	-10666.2
R(II)	-11004.0	497.8	-31.4	-43.6	-10581.2	464.3	-55. 5	-78.0	-10673.2
R(III)	-11002.9	500.6	-31.3	-43.6	-10577.3	468.3	-55.4	-78.0	-10668.0
TS	-10930.2	505.9	-30.9	-43.6	-10498.8	479.3	-54.6	-78.0	-10583.6
P(i)	-11005.0	499.1	-31.0	-43.6	-10580.5	466.6	-54.8	-78.0	-10671.2

Table S3. Individual contributions to the $\Delta A_{R(I)\rightarrow TS_B}$ and $\Delta A_{R(I)\rightarrow P(i)}$ terms (cf. Equation 4 in the main text) computed for type B isomerization of 2,4-dimethyl-pent-2-enium cation in the gas phase. All values are in kJ/mol.

	T=300 K		T=500 K	
	$R(I) \rightarrow TS_B$	$R(I) \rightarrow P(i)$	$R(I) \rightarrow TS_B$	$R(I) \rightarrow P(i)$
ΔA_{el}	70.4	-4.4	70.4	-4.4
ΔA_{vib}	6.0	-0.8	11.7	-1.1
ΔA_{rot}	0.3	0.3	0.6	0.6
ΔA_{trans}	0.0	0.0	0.0	0.0
$\boldsymbol{\Delta A_{total}}$	**76.8**	**-4.9**	**82.7**	**-5.0**
ΔU_{el}	70.4	-4.4	70.4	-4.4
ΔU_{vib}	-1.8	-0.6	-3.4	0.1
ΔU_{rot}	0.0	0.0	0.0	0.0
ΔU_{trans}	0.0	0.0	0.0	0.0
$\boldsymbol{\Delta U_{total}}$	**68.6**	**-5.0**	**67.0**	**-4.3**
$T\Delta S_{el}$	0.0	0.0	0.0	0.0
$T\Delta S_{vib}$	-7.8	0.2	-15.1	1.1
$T\Delta S_{rot}$	-0.3	0.2	-0.6	-0.5
$T\Delta S_{trans}$	0.0	0.0	0.0	0.0
$\boldsymbol{T\Delta S_{total}}$	**-8.1**	**0.0**	**-15.7**	**0.6**

SV.2. Type A isomerization

The reactant (and product) of type A isomerization has 6 equivalent stable rotamers. The dihedral angle θ between C^3-C^2-C^4-C^5 is -90 deg. for the first stable rotamer, and the five remaining rotational isomers are created by increasing θ by an integral multiple of increment $\Delta\theta$ =60 deg.

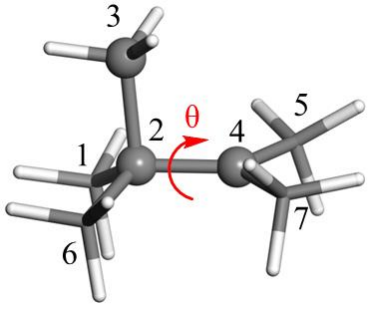

Figure S11. Numbering of the atoms of the first rotamer of P and dihedral angle θ (C^3-C^2-C^4-C^5).

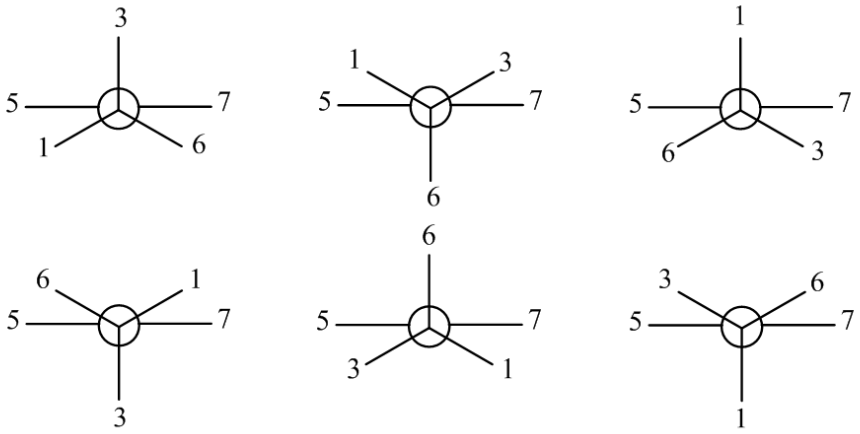

Figure S12. Schematic drawing showing six equivalent rotamers of the product P viewed along the direction parallel with the bond C^2-C^4 (cf. Figure S11).

Table S4. Individual contributions to the term $\Delta A_{P(i)\rightarrow TS_A}$ computed for type A isomerization of 2,3,3-trimethyl-but-2-enium cation in the gas phase. All values are in kJ/mol.

	$P(i) \rightarrow TS_A$	
	300 K	500 K
ΔA_{el}	13.7	13.7
ΔA_{vib}	1.0	2.5
ΔA_{rot}	0.0	0.1
ΔA_{trans}	0.0	0.0
$\boldsymbol{\Delta A_{total}}$	**14.7**	**16.2**
ΔU_{el}	13.7	13.7
ΔU_{vib}	-0.8	-2.1
ΔU_{rot}	0.0	0.0
ΔU_{trans}	0.0	0.0
$\boldsymbol{\Delta U_{total}}$	**12.9**	**11.6**
$T\Delta S_{el}$	0.0	0.0
$T\Delta S_{vib}$	-1.8	-4.6
$T\Delta S_{rot}$	0.0	-0.1
$T\Delta S_{trans}$	0.0	0.0
$\boldsymbol{T\Delta S_{total}}$	**-1.8**	**-4.7**

SVI. Static calculations of isomerization reactions in chabazite

In this section we provide numerical values of all contributions to the free energies of stable and transition states (Tables S5-S7, and S9-S11) and of selected structural parameters (Tables S8 and S12) for types B and A isomerizations in zeolite investigated using the static approach. Furthermore, structures of selected states are shown in Figures S14 and S15. Figure S13 shows the correlation between the electronic contribution to free energy of transition states TS_A and TS_B with the parameter χ defined in the main text (see Equation 6). For easier orientation the data for type B isomerization are presented in Section SVI.1 while those for type A isomerization in Section SVI.2.

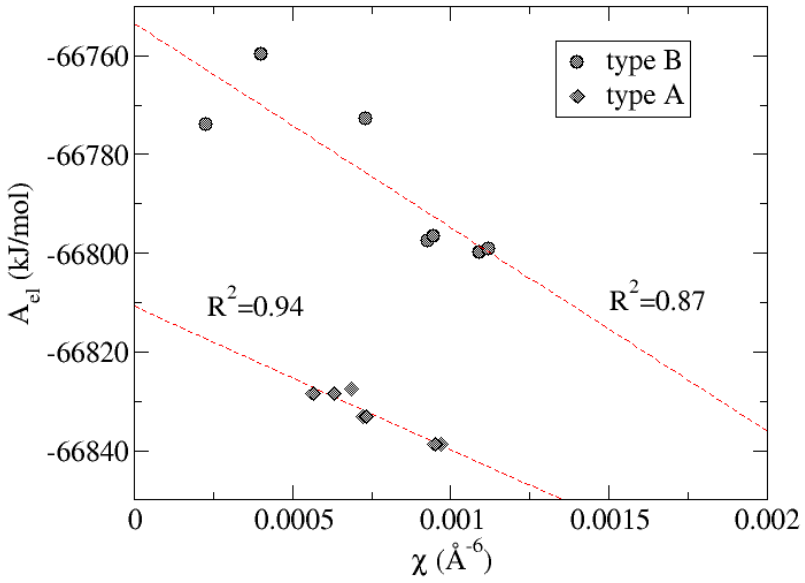

Figure S13. Correlation between the electronic contribution to free energy of TS_A and TS_B with sum of inverse distances between the framework Al and all C atoms raised to the power of six (χ). Dashed lines indicate the fitted linear functions and the corresponding correlation coefficients (R^2) are also shown.

SVI.1. Type B isomerization

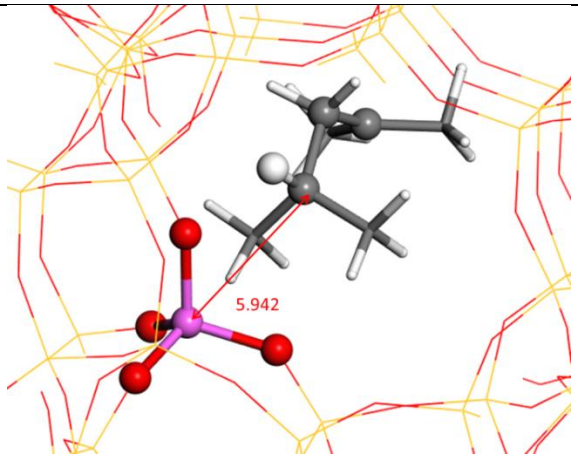

Reactant 1st configuration

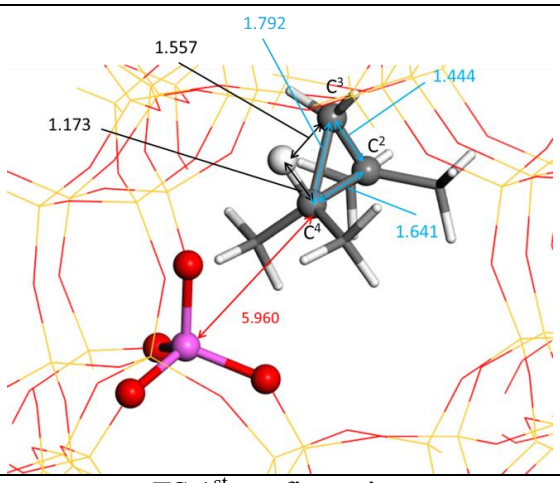

TS 1st configuration

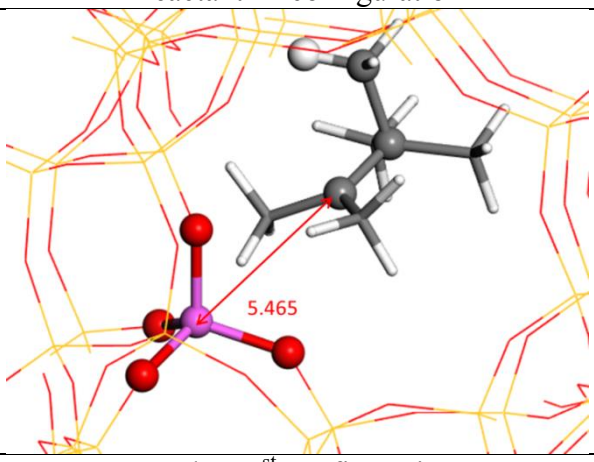

Product 1st configuration

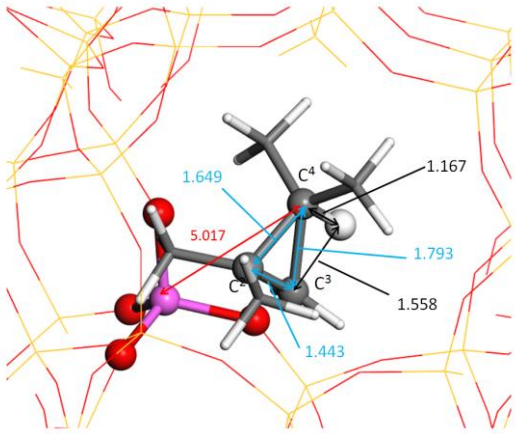

TS 2nd configuration

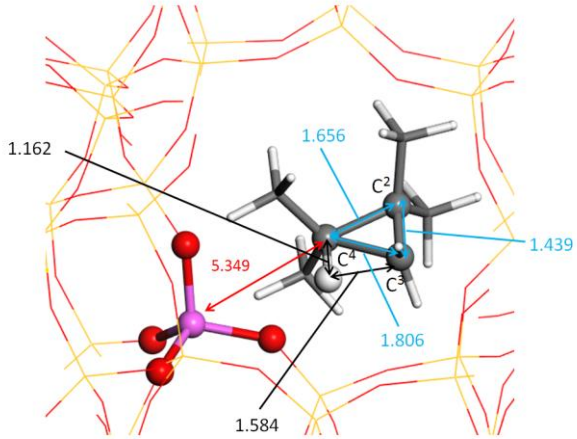

TS 3rd configuration

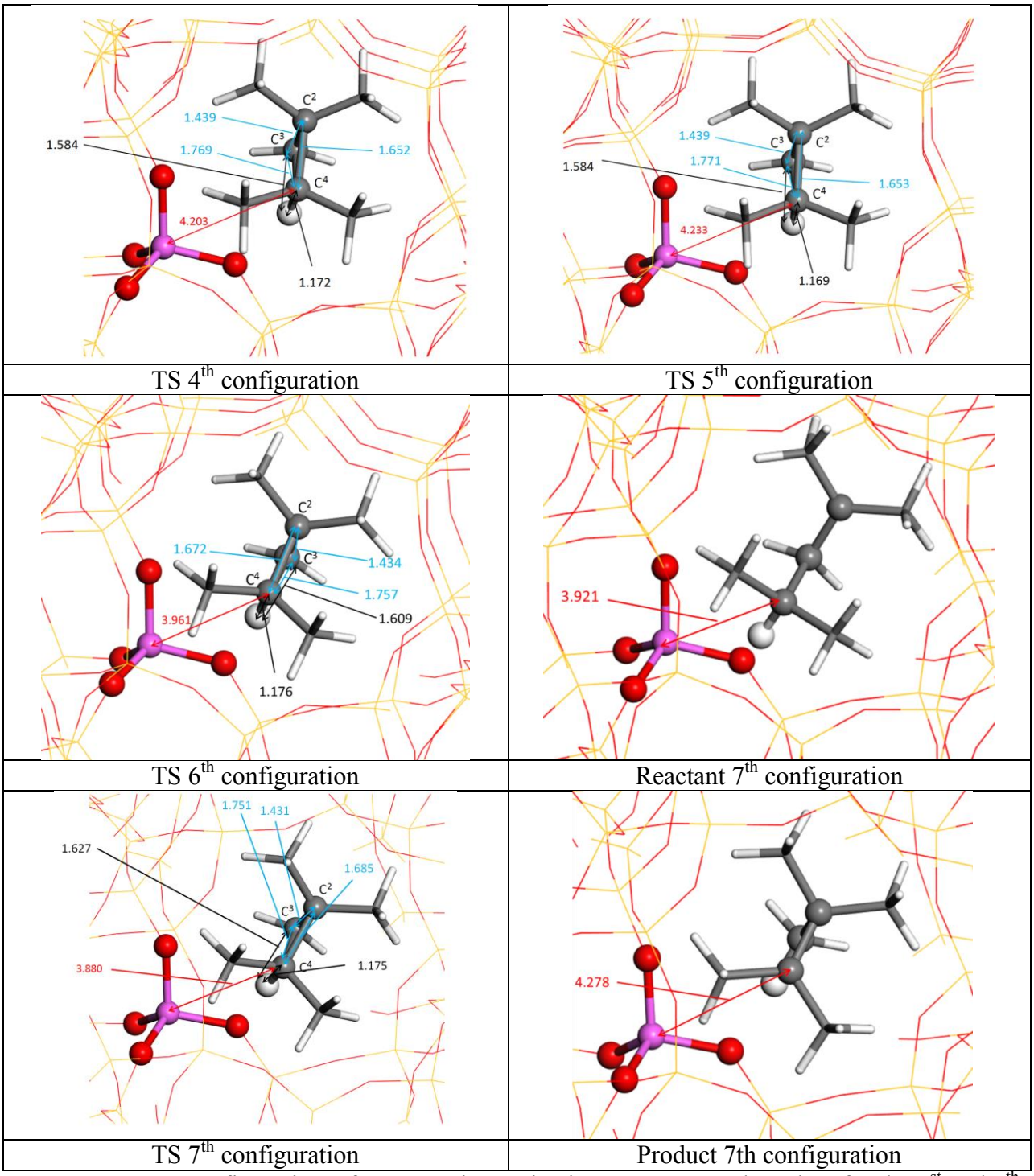

Figure S14. TS configurations, for type B isomerization. Reactant and product for the 1st and 7th configurations are also shown. Al in purple, H in white, Si in yellow and O in red. Selected interatomic distances are in Å.

Table S5. Helmholtz free energies computed using the static approach for seven transition state structures of type B isomerization reaction of 2,4-dimethyl-pent-2-enium cation in zeolite. Contributions of the electronic (A_{el}) and vibrational (A_{vib}) degrees of freedom to the total free energy (A_{tot}) of each state at 300 K and 500 K are indicated. All values are in kJ/mol.

Configuration	A_{el}	300 K		500 K	
		A_{vib}	A_{tot}	A_{vib}	A_{tot}
1	-66773.9	1034.6	-65739.6	701.8	-66072.3
2	-66772.6	1027.9	-65744.9	690.9	-66081.9
3	-66759.6	1027.6	-65732.2	690.0	-66069.8
4	-66797.4	1040.9	-65756.7	712.0	-66085.7
5	-66796.6	1039.5	-65757.3	709.6	-66087.2
6	-66799.8	1034.3	-65765.6	701.2	-66098.8
7	-66799.0	1027.3	-65771.9	689.4	-66109.8

Table S6. Helmholtz free energies computed using the static approach for the seven reactant (R(I)) and product (P) structures of type B isomerization reaction of 2,4-dimethyl-pent-2-enium cation in zeolite. Contributions of the electronic (A_{el}) and vibrational (A_{vib}) degrees of freedom to the total free energy (A_{tot}) of each state at 300 K and 500 K are indicated. All values are in kJ/mol.

Configuration	A_{el}	300 K		500 K	
		A_{vib}	A_{tot}	A_{vib}	A_{tot}
1 R(I)	-66842.2	1025.5	-65817.0	686.2	-66156.3
1 P	-66840.5	1018.3	-65822.4	674.4	-66166.3
2 R(I)	-66856.1	1026.9	-65829.4	688.8	-66167.6
2 P	-66845.6	1021.1	-65824.8	679.2	-66166.7
3 R(I)	-66832.9	1024.8	-65808.3	684.9	-66148.2
3 P	-66853.6	1029.0	-65824.9	692.5	-66161.3
4 R(I)	-66850.1	1029.6	-65820.7	692.3	-66158.0
4 P	-66858.8	1031.1	-65828.0	696.2	-66162.8
5 R(I)	-66850.1	1026.9	-65823.4	688.0	-66162.3
5 P	-66858.8	1032.8	-65826.2	699.1	-66159.9
6 R(I)	-66847.5	1022.7	-65825.0	681.3	-66166. 5
6 P	-66842.2	1026.5	-65815.9	686.3	-66156.0
7 R(I)	-66847.4	1025.7	-65821.9	685.3	-66162.3
7 P	-66842.4	1024.0	-65818.7	683.4	-66159.3

Table S7. Electronic (ΔA_{el}) and vibrational (ΔA_{vib}) contributions to the barriers $\Delta A_{R(I)\rightarrow TS_B}$ and $\Delta A_{P(i)\rightarrow TS_B}$ computed for type B isomerization of 2,4-dimethyl-pent-2-enium cation in zeolite. All values are in kJ/mol.

Configuration	ΔA_{el}	300 K		500 K	
		A_{vib}	ΔA_{tot}	ΔA_{vib}	ΔA_{tot}
1 R(I)→TS	68.3	9.1	77.4	15.6	84.0
1 P(i)→TS	66.6	16.3	82.8	27.5	94.0
2 R(I)→TS	83.5	1.0	84.5	2.2	85.7
2 P(i)→TS	73.0	6.8	79.8	11.7	84.8
3 R(I)→TS	73.2	2.8	76.0	5.2	78.4
3 P(i)→TS	94.0	-1.3	92.6	-2.5	91.5
4 R(I)→TS	52.7	11.3	64.0	19.7	72.4
4 P(i)→TS	61.4	9.9	71.2	15.8	77.1
5 R(I)→TS	53.5	12.6	66.1	21.7	75.2
5 P(i)→TS	62.3	6.7	69.0	10.5	72.8
6 R(I)→TS	47.7	11.6	59.3	19.9	67.7
6 P(i)→TS	42.4	7.9	50.3	14.9	57.3
7 R(I)→TS	48.4	1.6	50.1	4.1	52.5
7 P(i)→TS	43.5	3.3	46.8	6.0	49.5

Table S8. Lengths of the C-C and C-H bonds involved in the formation and the opening of the protonated cyclopropane, which is formed in the transition state of type B isomerization. All distances are in Å.

Configuration	d(Al-C^4)	d(C^4-C^3)	d(C^4-C^2)	d(C^2-C^3)	d(H^a-C^4)	d(H^a-C^3)
1	5.960	1.792	1.641	1.444	1.173	1.557
2	5.017	1.793	1.649	1.443	1.167	1.558
3	5.349	1.806	1.656	1.439	1.162	1.584
4	4.203	1.769	1.652	1.439	1.172	1.584
5	4.233	1.771	1.653	1.439	1.169	1.584
6	3.961	1.757	1.672	1.434	1.176	1.609
7	3.880	1.751	1.685	1.431	1.175	1.627

S.VI.2. Type A isomerization

Table S9. Helmholtz free energies computed using the static approach for seven transition state structures of type A isomerization reaction of 2,3,3-trimethyl-but-2-enium cation in zeolite. Contributions of the electronic (A_{el}) and vibrational (A_{vib}) degrees of freedom to the total free energy (A_{tot}) of each state at 300 K and 500 K are indicated. All values are in kJ/mol.

Configuration	A_{el}	300 K		500 K	
		A_{vib}	A_{tot}	A_{vib}	A_{tot}
1	-66833.1	1033.7	-65799.4	699.1	-66134.0
2	-66828.4	1031.9	-65796.5	696.7	-66131.7
3	-66828.4	1029.5	-65798.9	693.2	-66135.2
4	-66827.5	1020.4	-65807.1	678.4	-66149.1
5	-66838.6	1030.3	-65808.3	693.8	-66144.8
6	-66833.1	1032.2	-65800.9	696.7	-66136.4
7	-66838.6	1031.4	-65807.2	695.6	-66143.0

Table S10. Helmholtz free energies computed using the static approach for reactant/product structures of type A isomerization reaction of 2,3,3-trimethyl-but-2-enium cation in zeolite. Contributions of the electronic (A_{el}) and vibrational (A_{vib}) degrees of freedom to the total free energy (A_{tot}) of each state at 300 K and 500 K are indicated. All values are in kJ/mol.

Configuration	A_{el}	300 K		500 K	
		A_{vib}	A_{tot}	A_{vib}	A_{tot}
1	-66860.9	1026.4	-65834.5	688.2	-66172.7
	-66842.0	1029.9	-65812.1	692.8	-66149.2
2	-66846.4	1026.3	-65820.1	687.1	-66159.3
	-66857.3	1031.4	-65825.9	695.7	-66161.6
3	-66839.8	1028.6	-65811.2	690.7	-66149.1
	-66858.2	1022.1	-65836.1	680.4	-66177.8
4	-66843.9	1028.0	-65815.9	689.7	-66154.2
	-66854.9	1024.2	-65830.7	684.1	-66170.8
5	-66848.3	1030.5	-65817.8	694.2	-66154.1
	-66854.0	1029.0	-65825.0	691.5	-66162.5
6	-66842.0	1029.8	-65812.2	692.6	-66149.4
	-66860.9	1028.7	-65832.2	692.0	-66168.9
7	-66854.1	1031.5	-65822.6	695.6	-66158.5
	-66848.3	1029.6	-65818.7	692.5	-66155.8

Table S11. Electronic (ΔA_{el}) and vibrational (ΔA_{vib}) contributions to the barrier $\Delta A_{P(i)\rightarrow TS_A} \equiv \Delta A_{tot}$ computed for type A isomerization of 2,3,3-trimethyl-but-2-enium cation in zeolite. All values are in kJ/mol.

Configuration	ΔA_{el}	300 K		500 K	
		ΔA_{vib}	ΔA_{tot}	ΔA_{vib}	ΔA_{tot}
1	27.8	7.3	35.0	10.9	38.6
	8.9	3.8	12.7	6.3	15.2
2	18.0	5.6	23.6	9.7	27.7
	28.9	0.5	29.4	1.0	29.9
3	11.4	0.9	12.3	2.4	13.8
	29.8	7.4	37.2	12.8	42.6
4	16.4	-7.7	8.7	-11.3	5.1
	27.4	-3.8	23.6	-5.6	21.8
5	9.7	-0.2	9.5	-0.3	9.3
	15.4	1.3	16.8	2.4	17.8
6	8.9	2.4	11.3	4.0	12.9
	27.8	3.4	31.3	4.6	32.5
7	15.5	-0.1	15.3	0.0	15.5
	9.7	1.8	11.5	3.0	12.7

Table S12. The interatomic distances Al-C^4 and Al-C^2, and the lengths of the C-C bonds involved in the formation and the opening of the protonated cyclopropane in the transition state of the type A isomerization. All distances are in Å.

Configuration	d(Al-C^4)	d(Al-C^2)	d(C^4-C^2)	d(C^4-C^3)	d(C^2-C^3)
1	5.912	4.560	1.421	1.886	1.768
2	4.510	4.968	1.419	1.830	1.870
3	5.470	4.526	1.420	1.895	1.805
4	4.617	5.994	1.422	1.818	1.874
5	5.386	4.213	1.419	1.848	1.795
6	5.905	4.550	1.421	1.885	1.769
7	5.412	4.225	1.419	1.846	1.801

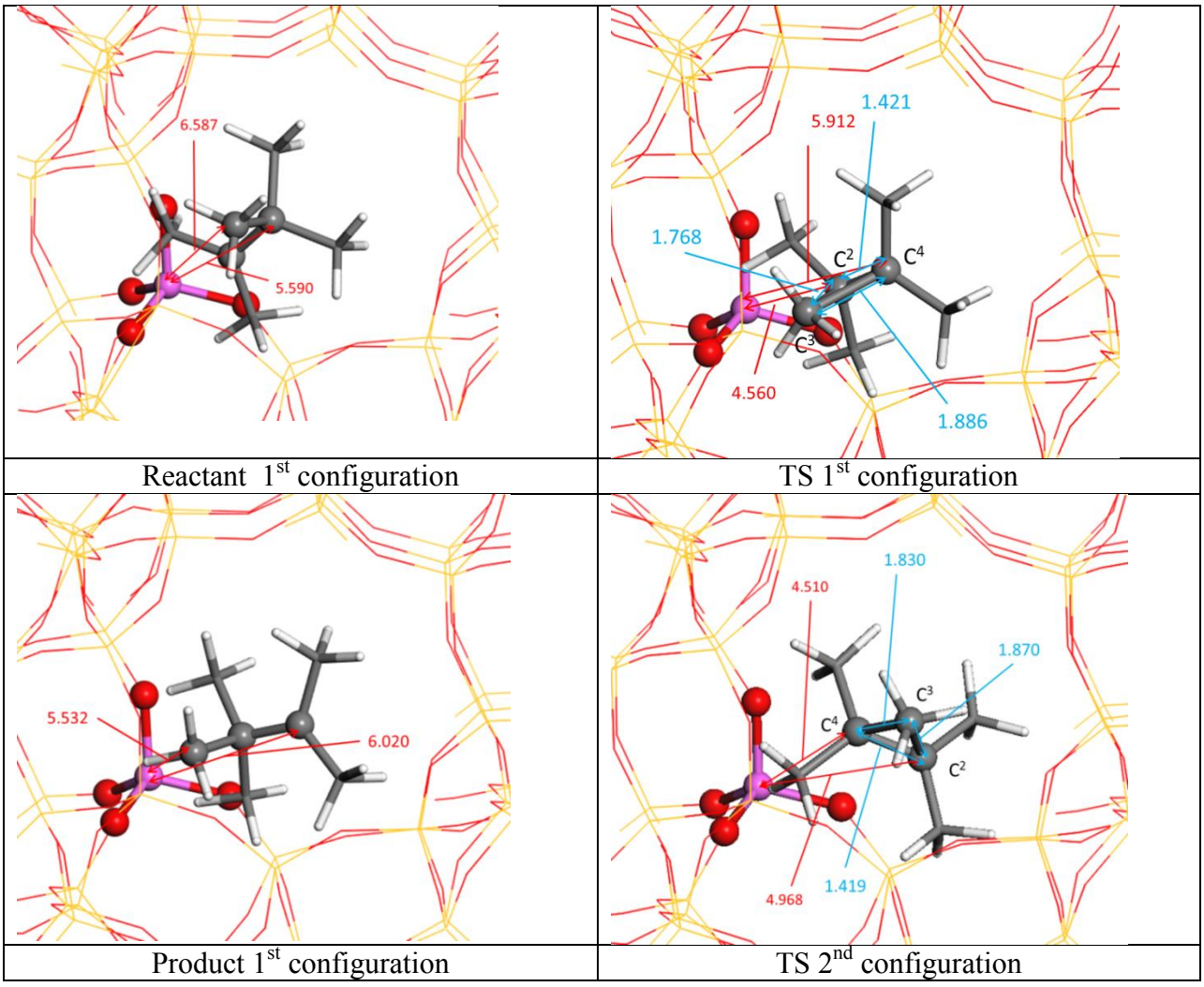

Reactant 1st configuration	TS 1st configuration
Product 1st configuration	TS 2nd configuration

Figure S15. Selected reactant, product, and TS configurations, for type A isomerization. Al in purple, H in white, Si in yellow and O in red. Selected interatomic distances are in Å.

SVII. Additional structural MD data

SVII.1. Analysis of the C-C bonds involved in the PCPs

The probability distribution functions for the three C-C bonds (C^2-C^3, C^3-C^4 and C^2-C^4) involved in the reactions determined using the data generated by MD of reactant, transition state, and product states are shown in Figures S13-S16. These distributions were fitted by the Gaussian function:

$$f(d) = \frac{1}{\sqrt{2\pi\sigma^2}} exp\left(-\frac{(d-\mu)^2}{2\sigma^2}\right). \quad \text{(Eq. S6)}$$

Assuming that each bond (d) can be represented by a harmonic oscillator with the force constant κ, the standard deviation (σ) of the corresponding distribution can be identified [6] with the term $\sqrt{\frac{k_B T}{\kappa}}$. Hence the relative strength of the bond can be estimated from the width of the corresponding probability distribution. The parameter μ stands for the average value of the bond. The values of fitting parameters μ and σ are presented in Table S13.

Table S13. The parameters μ and σ (in Å) obtained by fitting the MD data for the reactant (R(I)), transition state (TS_B), and product (P) configurations of type B isomerization, and transition state (TS_A) for type A isomerization by Equation S6. Note that P is also the reactant/product of type A isomerization.

		T = 300 K		T = 500 K	
bond	species	μ	σ	μ	σ
C^2-C^3	R(I)	1.45168	0.0328534	1.45361	0.0415915
C^2-C^4	R(I)	2.53987	0.0807952	2.56763	0.106345
C^3-C^4	R(I)	1.62466	0.0529897	1.62719	0.0722078
C^2-C^3	TS_B	1.44327	0.0296228	1.44745	0.037927
C^2-C^4	TS_B	1.66545	0.0496497	1.66697	0.0643271
C^3-C^4	TS_B	1.77854	0.0567455	1.80294	0.0710366
C^2-C^3	P	1.60597	0.0481422	1.62574	0.067394
C^2-C^4	P	1.47203	0.0339286	1.46641	0.0451147
C^3-C^4	P	2.31329	0.0927257	2.28838	0.133306
C^2-C^4	TS_A	1.42161	0.0268869	1.42394	0.0329199
C^3-C^4	TS_A	1.85121	0.0601533	1.87182	0.0868662
C^2-C^3	TS_A	1.84396	0.0591849	1.86382	0.083486

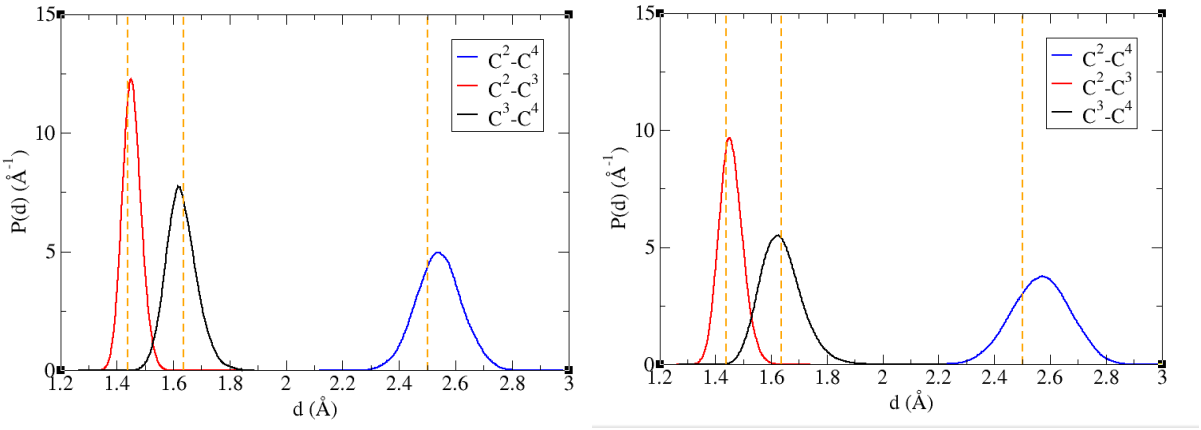

Figure S16. Probability distribution functions (solid lines) for the C-C bonds (d) in reactant R(I) of type B isomerization at T = 300 K (left) and T=500 K (right). Dashed lines indicate results from the static approach applied to the reaction in the gas phase.

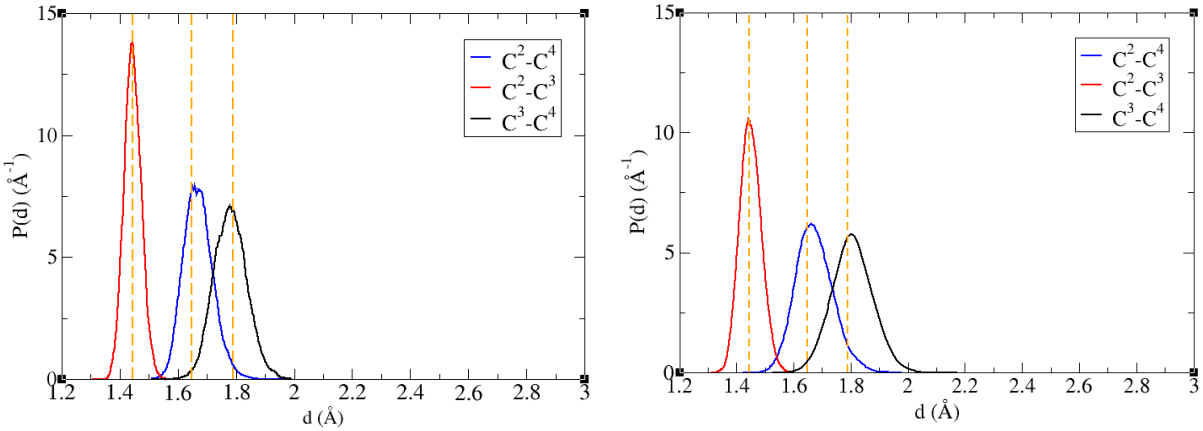

Figure S17. Probability distribution functions (solid lines) for the C-C bonds (d) in the transition state TS_B of type B isomerization at T = 300 K (left) and T=500 K (right). Dashed lines indicate results from the static approach applied to the reaction in the gas phase.

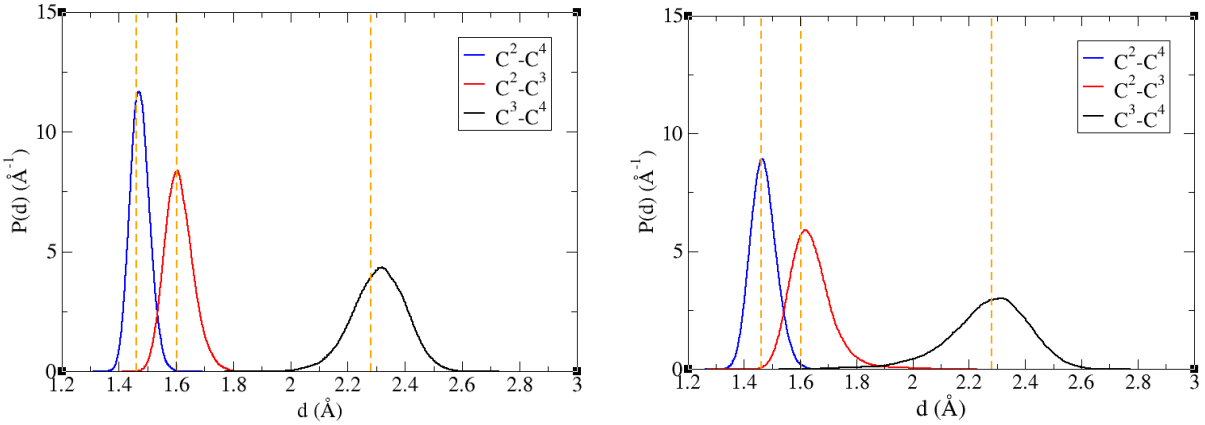

Figure S18. Probability distribution functions (solid lines) for the C-C bonds (d) in the product P of type B isomerization at T = 300 K (left) and T=500 K (right). Dashed lines indicate results from the static approach applied to the reaction in the gas phase. Note that P is also the reactant/product for type A isomerization.

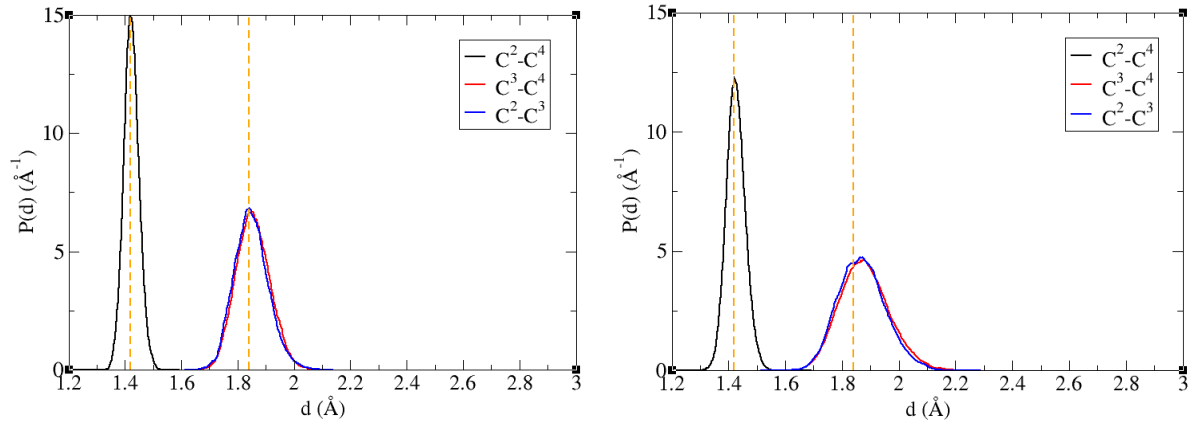

Figure S19. Probability distribution functions (solid lines) for the C-C bonds (d) in the transition state TS_A of type A isomerization at T = 300 K (left) and T=500 K (right). Dashed lines indicate results from the static approach applied to the reaction in the gas phase.

SVII.2. Fluctuation of potential energy

An example of the potential energy distribution $\delta E = E_p - \langle E_p \rangle$ computed for the free energy transition state of type B isomerization is shown Figure S20. As expected, the distribution is much broader than the potential energy differences between individual TS configurations identified in our static calculations (within around 40 kJ/mol, see Sec. 3.2. in the main text). This behavior is a natural consequence of thermal fluctuations of a many-body system.

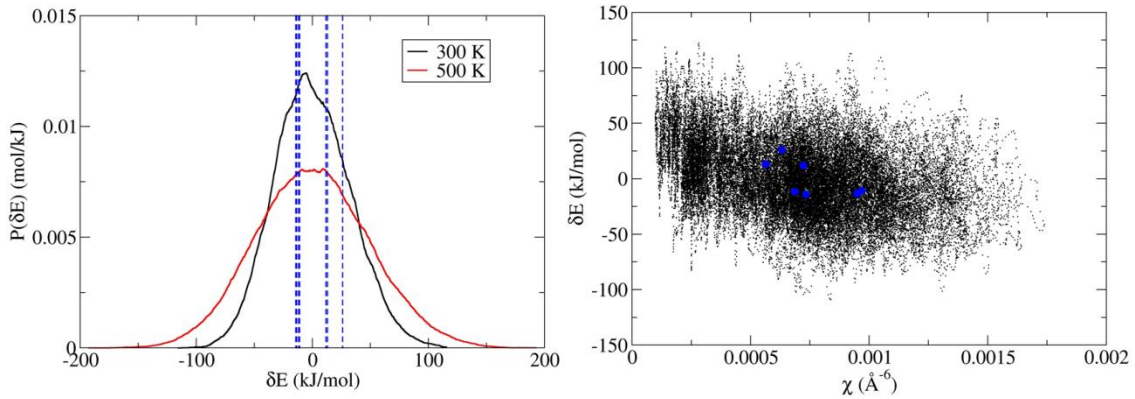

Figure S20. Left: probability distribution function for the fluctuation of potential energy $\delta E = E_p - \langle E_p \rangle$ for the TS of type B isomerization at 300 K and 500 K. The values of δE determined in the static approach are indicated by vertical dot lines. Right: same fluctuation δE at 300 K as a function of χ (equation 6 in the main text). The values determined in the static approach are indicated by blue dots.

References

[1] E.A. Carter, G. Ciccotti, J.T. Hynes, R. Kapral, Chem. Phys. Lett. 156 (1989) 472–477.
[2] C. Dellago, P.G. Bolhuis, P.L. Geissler, Advances in Chemical Physics 123 (2002).
[3] B. Peters, Annual review of physical chemistry 67 (2016) 669–690.
[4] T. Bučko, J. Phys-Condens. Matter 20 (2008) 64211.
[5] G. Ciccotti, M. Sprik, J. Chem. Phys. 109 (1998) 7737–7744.
[6] R. Baron, W.F. van Gunsteren, P.H. Hünenberger, Trends Phys. Chem. 11 (2006) 87–122.
[7] B. Peters, J. Chem. Phys. 125 (2006) 241101.